A STUDY ON MANEUVERABILITY OF VLCC INSTALLED WITH MARINER TYPE VEC-TWIN RUDDER

Dong-Hoon Kang (Osaka University, Japan)
Kazuhiko Hasegawa (Osaka University, Japan)
Kenjiro Nabeshima (Japan Hamworthy Co. Ltd)

Abstract: Maneuverability of VLCC installed with mariner type Vec-twin rudder is studied in this paper. Mathematical model of mariner type Vec-twin rudder is developed for maneuvering simulation of a large vessel. The coefficients of interaction between hull and rudder (t_R, a_H, x_H) were obtained from self propulsion test with a 4m VLCC ship model fitted with mariner type Vec-twin rudder. Forces acting on both rudders with rotating propeller were also measured during the self propulsion test. Hydrodynamic coefficients were estimated based on a published regression formula to develop maneuvering simulation. Free running tests such as Turning and Zigzag tests were carried out with same model ship and rudder which was tested in towing tank. The results were compared with the simulations to modify and validate mathematical models of the hull and the mariner type Vec-twin rudder.

During self propulsion tests it was observed that flow to the mariner type Vec-twin rudder is not parallel to ship's center line. Virtual zero rudder angle concept is applied to improve the maneuverability of the ship with the mariner type Vec-twin rudder. Simulations using "virtual zero rudder angle" and "zero rudder angle" respectively, were carried out. The results of the simulation were compared from the points of view of maneuverability and asymmetrical maneuvering motions.

1. INTRODUCTION

Blunt body ships such as VLCC have lower maneuverability as compared to fine form ships, because of their hull form which is designed for higher loading. After the IMO standards for ship maneuverability [1] were adopted in 2002, many efforts have been made to improve the maneuverability of these ships. Utilizing special controller is one of the ways of increasing ship's maneuverability. The special control system may perform excellently in certain circumstances, but the controllers can not increase the inherent maneuverability of a ship, and the control system cannot be used while carrying out maneuverability tests as per IMO standards. Moreover, some existing large sized vessels, which otherwise have been well proven in real voyage, do not satisfy the IMO Standards for ship maneuverability, especially stopping ability. Using special rudder systems is one of the alternatives for increasing the inherent maneuverability of such vessels. Small and medium sized vessels installed with super Vec-twin rudder show better stopping ability and maneuverability than those installed with conventional rudder [2], but large diameter rudder stocks and special design of stern are required while using super Vec-twin rudders on large vessels. Mariner type super Vec-twin rudder has been proposed as one of the special rudder systems for solving the above problem. Its performance in maneuvering motion is comparable to conventional mariner rudder, while stopping ability is superior to mariner rudder [3].

The Mariner type super Vec-twin rudder (hereinafter MSV rudder)* is a new type of rudder, its performance and characteristic have not been defined clearly. Since the MSV rudder employs horizontal fins to improve ship's propulsion, the interaction from the fins may make some difficulties during analysis. In this paper, the Mariner type Vec-twin rudder (hereinafter MVT rudder) which has the same shape as that of the MSV rudder without horizontal fins, is studied to define the characteristics of the MSV rudder as first step. A typical MVT type rudder is shown in Figure 1.

Self propulsion tests of the VLCC model ship with MVT rudder were carried out for assessing the performance of the MVT rudder on large vessels. A mathematical model for MVT rudder was developed based on the measured force on MVT rudder from the experiments. The maneuvering simulation of the VLCC model ship was also developed based on MMG model to figure out the performance of the MVT rudder on a maneuvering ship.

* US 6,886,485 B2: Twin-Rudder System for Large Ship

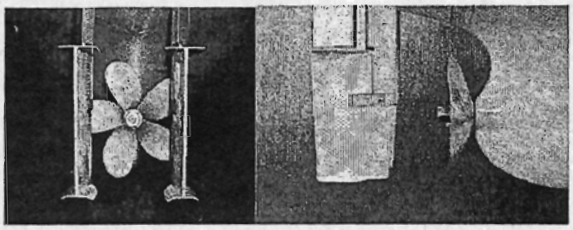

Fig.1 Shape of MVT rudder

2. MODEL EXPERIMENT

Model experiments of MVT rudder in the towing tank were carried out for measuring hydrodynamic performance of the rudder. The performances of the rudder at various rudder angles were measured behind a hull and a propeller. A 4m VLCC model ship was chosen for this study. Particulars of the model ship are shown in Table 1.

Table 1 Principal dimensions of model ship

L	4.00m	x_G	0.123m
B	0.667m	S_W	4.049m^2
d	0.240m	D_P	0.12057m
C_b	0.817	A_R / Ld	1/71.0

Four sets of experiment were carried out with various rudder angles. The rps of the propeller was set at 13.7 and 7.0 respectively, they correspond to Full speed and Slow speed of the ship. The speeds of ship were set corresponding to surge speed which is expected during maneuvering condition such as Turning. The conditions of the experiments are shown Table 2. It may be noted that graphs which show the results of the analysis use either J_S or S to represent each set of the experiment for easy understanding.

Table 2 Conditions of experiments

Speed (m/s)	rps	J_S	S
0.8	13.7	0.484	0.557
0.4	13.7	0.242	0.749
0.4	7	0.474	0.564
0.2	7	0.237	0.753

2.1 Mathematical Model of Rudder Force

To express the hydrodynamic forces and moment due to the MVT rudder, Hamamoto's expression [4] is used. The sum of the forces generated by each rudder was considered as single force, and the interactions between a hull and two rudders were described with a set of coefficients. Hydrodynamic forces and moment due to the rudders are expressed as Equation 1.

$$\left.\begin{aligned} X_R &= -(1-t_R)(F_{NS}\sin\delta_S + F_{NP}\sin\delta_P) \\ Y_R &= -(1+a_H)(F_{NS}\cos\delta_S + F_{NP}\cos\delta_P) \\ N_R &= -(x_R + a_H x_H)(F_{NS}\cos\delta_S + F_{NP}\cos\delta_P) \end{aligned}\right\} \quad (1)$$

2.2 Interaction between Hull and Rudder

To obtain the coefficients of the interaction between the hull and the rudders (t_R , a_H , x_H), the measured data were analyzed based on the Equation 1. The terms in Equation 1 can be simplified to equation 2.

$$\left.\begin{aligned} F_{N\sin} &= F_{NS}\sin\delta_S + F_{NP}\sin\delta_P \\ F_{N\cos} &= F_{NS}\cos\delta_S + F_{NP}\cos\delta_P \end{aligned}\right\} \quad (2)$$

Figure 2 shows the relation between X_H , X_p and X_R . The vertical axis is the sum of rudder forces and the horizontal axis is the rudder forces acting on the hull. Therefore, the gradient of the data on graph represents $1-t_r$. The result shows the gradients of each set of the experiment does not significantly depend on J_s and the gradients from all the experiment had similar values. So, t_r was considered as constant value.

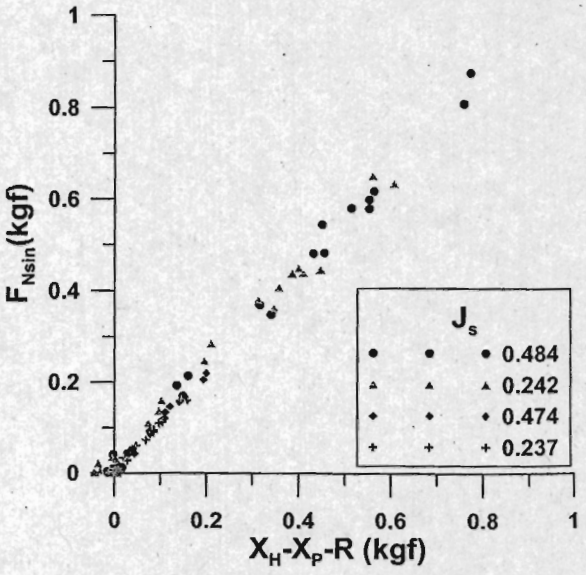

Fig.2 Interaction between hull, propeller and rudder in surge direction

The interaction between the hull and the rudders in the sway direction is shown in Figure 3. The same way of analysis was carried out as described earlier. But, the gradient, which represents a_H , in the four graphs are different, contrary to earlier result for t_r in surge direction. a_H was drawn against J_S and is shown in Figure 4. Three different speeds and two different rps were chosen for the experiments, but the values of J_S were not spread out. It was difficult to figure out a trend of a_H only with the tested conditions. Therefore the assumption that a_H

is nearly 0 value when the value of J_S is close to 0 was set and plotted in Figure 4. The values of a_H were fitted as a second order polynomial and were represented as equation 3.

$$a_H = a_1 J_S + a_2 J_S^2 \tag{3}$$

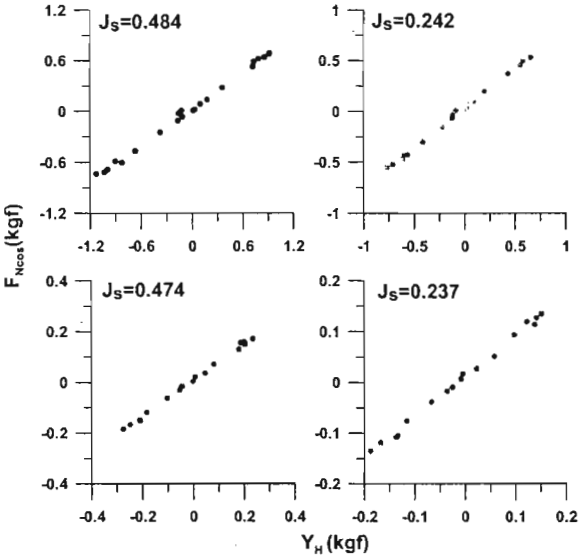

Fig.3 Interactions between hull, propeller and rudder in sway direction

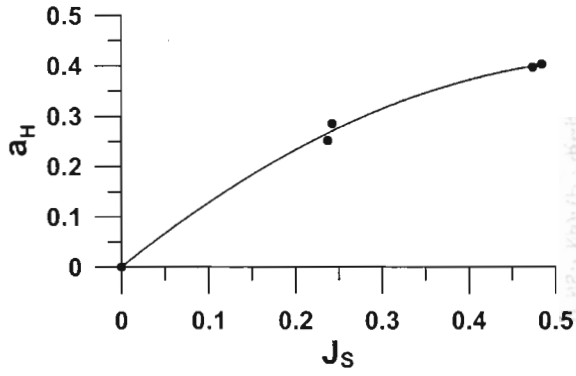

Fig.4 Interaction coefficient a_H

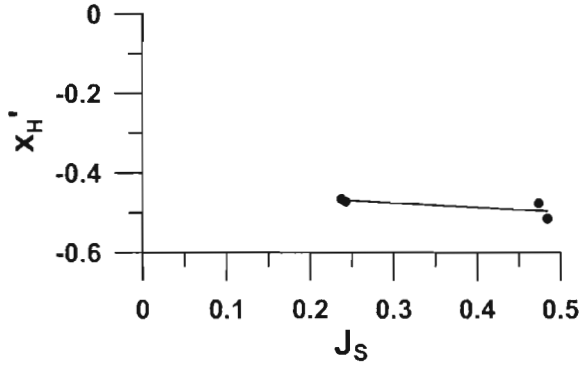

Fig.5 Interaction coefficient x_H'

x_H' was calculated in the same way as a_H and is shown in Figure 5. The change of x_H' was not significant as compared to a_H, and was fitted with a linear term. The change of x_H' on J_S is defined as Equation 4.

$$x_H' = b_1 + b_2 J_S \tag{4}$$

2.3 Inflow Angle to MVT Rudder

A conventional Mariner rudder is installed right behind a propeller at the center of a ship. It is expected that the angle of the propeller slip steam to the mariner rudder is nearly zero. On the other hand, MVT rudder system has a propeller and two rudders, and the rudders are installed away from the center of the ship symmetrically. The flow speeds between two rudders and outside of the rudders are different. A sketch of inflow to MVT rudder is shown in Figure 6. The flow stream (B) which is directly accelerated by the propeller should be faster than the flow streams (A) and (C). Because of the above reason, the inflow angles to the rudders should have a certain angle in contrast to the Mariner rudder.

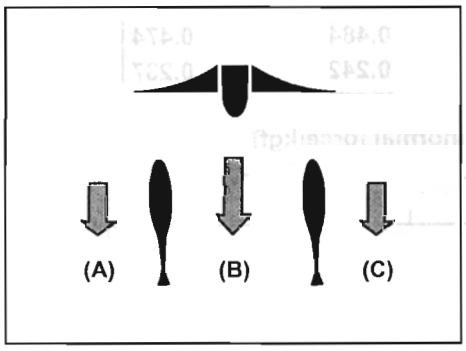

Fig.6 Sketch of inflow to MVT rudder

Figure 7 and Figure 8 show the measured normal force on starboard and port side rudders, respectively. It is observed that $|\delta_{S0}|$ and $|\delta_{P0}|$ are about 5 degrees for the steady condition where the propeller force matches with ship's resistance. $|\delta_{S0}|$ and $|\delta_{P0}|$ are further increased when ship's speed is down with the same rps, this represents the acceleration condition. With these results, it can be concluded that $|\delta_{S0}|$ and $|\delta_{P0}|$ increases when the ratio of the flow speed (B) and the flow speeds (A) (C) increases. Therefore δ_{S0} and δ_{P0} can be expressed as a function of propeller slip ratio S. The δ_{S0} and δ_{P0} were calculated by fitting the rudder normal forces, and are shown in Figure 9. It may be noted that since the experiments were not carried out for various values of S, the δ_{S0} and δ_{P0} were assumed as zero when S is zero, and plotted in Figure 9. It is doubtful that the δ_{S0} and δ_{P0} change linearly with the change of S, but that was assumed because of lack of the data.

$$\left.\begin{aligned} \delta_{S0} &= C_1 S \\ \delta_{P0} &= C_2 S \end{aligned}\right\} \tag{5}$$

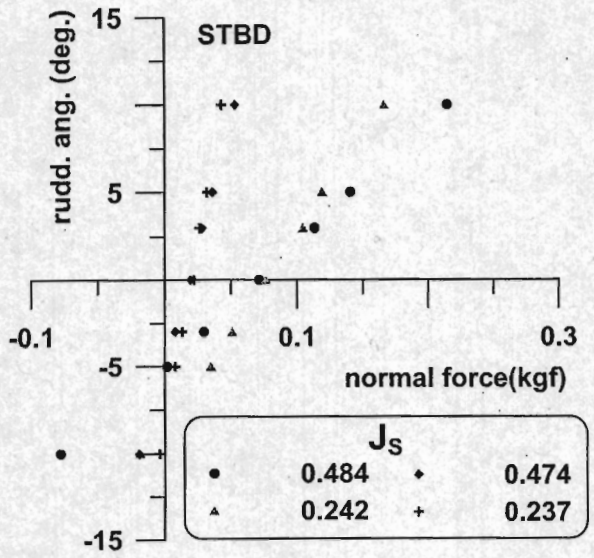

Fig.7 Normal force of starboard side rudder at small rudder angle

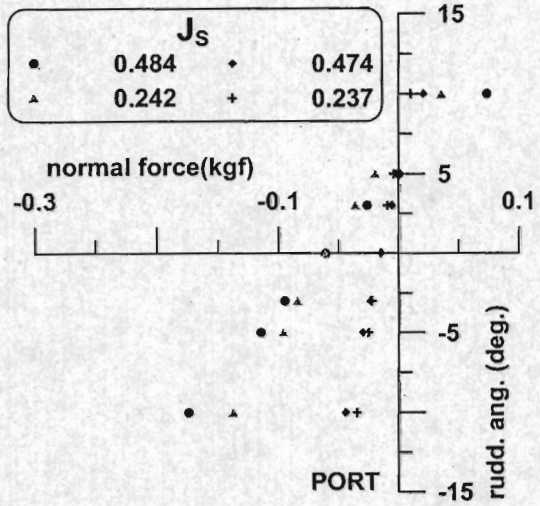

Fig.8 Normal force of port side rudder at small rudder angle

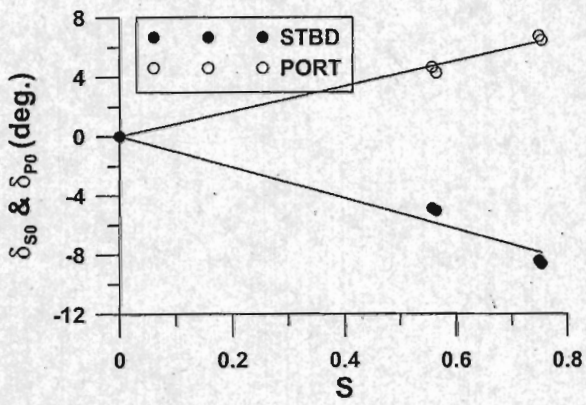

Fig.9 Trends of δ_{S0} and δ_{P0} of MVT rudder

2.3 Prediction of Normal Coefficient of Rudder

Since rudder open water test for the MVT rudder were not carried out, the normal force coefficient is estimated by analyzing the rudder force behind propeller. It is possible to predict the inflow speed (B) in Figure 6 using the conventional mathematical model such as Equation 6.

$$\left.\begin{aligned} u_R &= \frac{\varepsilon u_P}{1-s}\sqrt{\eta\left[1+\kappa\left(\sqrt{1+\frac{8K_T}{\pi J_P^2}}-1\right)\right]^2+(1-\eta)} \\ u_P &= (1-\omega_P)u \\ \kappa &= kx/\varepsilon \\ \eta &= D_P/h_R \end{aligned}\right\} \quad (6)$$

When the angles of the two rudders are small, it is assumed that the interaction between two rudders can be neglected. The cases of the experiment which have small rudder angle to tail inboard with high speed of the ship and rps were chosen, and the rudder normal forces are non-dimensionalized with the inflow speed that is the equation 6. This is because, when the rudders are turned inboard, most of the rudder area is in way of the propeller slipstream, and the slipstream around the rudder can be predicted by the equation 6. Figure 10 shows the non-dimensionalized rudder forces in the above condition.

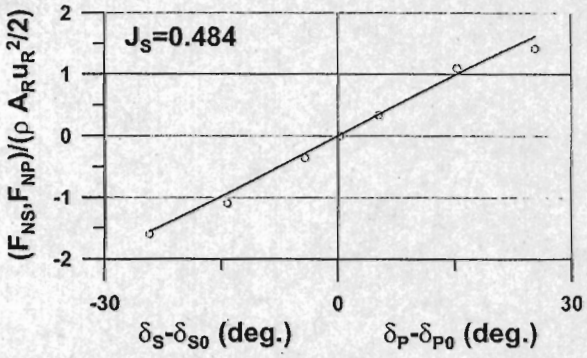

Fig.10 Non-dimensional normal forces at small rudder angle

The gradient in Figure 10 is used as the rudder normal coefficient CN for the MVT rudder. The calculated CN was 3.8 which is 1.32 times of that of the mariner rudder which has the same aspect ratio calculated by Fujii's formula [5]. When the dimensions of the Schilling rudder and the normal rudder are the same, the normal force coefficient for the Schilling rudder can be approximately expressed from that of normal rudder by multiplying it by 1.3 [6]. The cross section of the MVT rudder is the same as that of a Schilling Rudder. From the above, it can be concluded that the calculated rudder normal coefficient reasonably expresses the forces of the MVT rudder.

2.4 Formulations of Inflow Speed to Rudder

The inflow speeds to the rudders are calculated by analyzing the measured rudder forces. The inflow speeds in the condition which have small rudder angle to inboard were calculated as per Equation 6. The inflow speeds without the above condition were calculated as per Equation 7.

$$\left.\begin{aligned} u_{RS} &= \sqrt{F_{NS} \Big/ \{\rho A_R C N \sin\alpha_S / 2\}} \\ u_{RP} &= \sqrt{F_{NP} \Big/ \{\rho A_R C N \sin\alpha_P / 2\}} \\ \alpha_S &= \delta_S - \delta_{S0} \\ \alpha_P &= \delta_P - \delta_{P0} \end{aligned}\right\} \quad (7)$$

The ratio of the inflow speeds which were calculated by the equation 6 and 7 are shown in Figure 11 and Figure 12 respectively. The drop of the inflow speeds at (A) and (C) is shown in Figure 11. The values at left side are the drop of the inflow to the port side rudder when the effective rudder angles α_P are below zero, and those at right side are for the starboard side rudder with positive α_S. It is observed that the inflow speeds dropped corresponding to the effective rudder angles α_S and α_P. The drop of the inflow speed were analyzed as functions of α_S, α_P and S as shown in Equation 8. It may be noted that the decrease in rudder lift due to the stall at large rudder angle were also considered as the drop of the inflow speed. This is due to the fact that commencement of the stall when rudder is behind a propeller is difficult to define [7], and the effect of the stall is represented as the effect of the drop of the inflow speed.

$$\left.\begin{aligned} u_{RS} &= u_R \cdot \left(A_S \alpha_S^2 + C_S\right) \quad at\ \alpha_S > 0 \\ u_{RP} &= u_R \cdot \left(A_P \alpha_P^2 + B_P \alpha + 0.96\right) \quad at\ \alpha_P < 0 \\ A_S &= -0.35S + 0.164S^2 \\ C_S &= 1 - 0.1170S^2 \\ A_P &= 0.247S + 0.206S^2 \\ B_P &= 0.203S + 0.57S^2 \end{aligned}\right\} \quad (8)$$

Figure 12 shows the increment of the inflow speed due to the interaction of the two rudders. The conditions of the experiments are that one side rudder was set at 30 degrees to tail inboard and the other side rudder was set at 30, 45 and 60 degrees to tail outboard. It is observed that the inflow speed to a rudder is increased when the other side rudder is turned to outboard with large rudder angles. Contrary to Figure 11, in this case it was difficult to observe

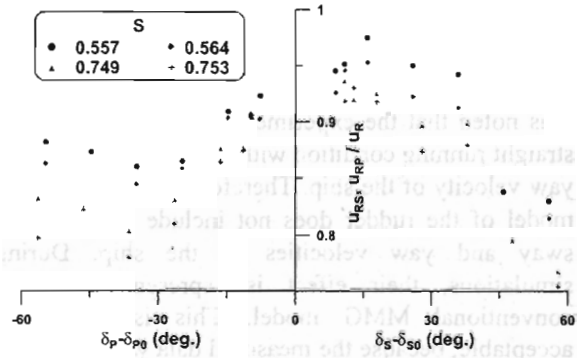

Fig.11 Drops of inflow speeds to port and starboard rudders

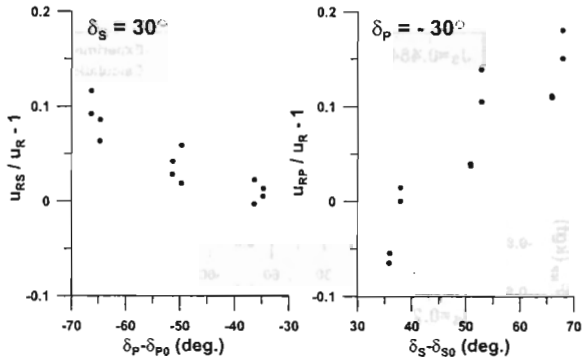

Fig.12 Effect of interaction between two rudders

dependence on S. So the conditions of the experiments were not distinguished in Figure 12, and the changes in the inflow speed due to the interaction are analyzed with a function of α_S or α_P as shown in Equation 9. It is noted that the interaction between two rudders when the angles of rudders are small was disregarded. This is because the rudder forces with small angles were themselves very small, so it was difficult to figure out the effect of the interaction.

$$\left.\begin{aligned} u_{RS} &= u_R \cdot \left\{1 + 0.239 \cdot \left(\alpha_P + \pi/6\right)^2\right\} \\ &at\ \alpha_S < 0\ \&\ \alpha_P < 30° \\ u_{RP} &= u_R \cdot \left\{1 + 0.362 \cdot \left(\alpha_S - \pi/6\right)^2\right\} \\ &at\ \alpha_P > 0\ \&\ \alpha_S > 30° \end{aligned}\right\} \quad (9)$$

2.5 Validating Mathematical Model of Rudder Force

The calculations with the developed rudder model were carried out at the same condition of the experiments. Figure 13 shows the example of the comparison of rudder forces between the experiment and the calculation when the two rudders have the same rudder angle i.e. when they are parallel. Although the experiment and the calculation have small deviation at large rudder angles, generally the calculation well describes the experiment data. From

the above results, it can be concluded that the proposed mathematical rudder model is suitable for expressing the forces of the MVT rudder.

It is noted that the experiments were carried out on straight running condition without any drift angle and yaw velocity of the ship. Therefore the mathematical model of the rudder does not include the effect of sway and yaw velocities of the ship. During simulations, their effect is represented by the conventional MMG model. This is considered acceptable, because the measured data were analyzed based on MMG type mathematical model for describing the performance of the rudder.

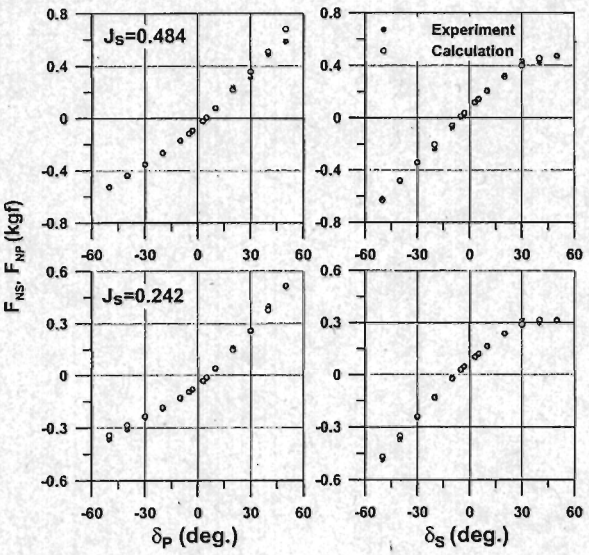

Fig.13 Comparisons of rudder forces between experiment and calculation at parallel rudder angle

3. SIMULATION OF MANEUVERING SHIP

Equations of a maneuvering ship are written as per MMG model. The mathematical model of ship's maneuvering motion is described based on three degrees of freedom, surge, sway and yaw motion. The equations of the ship maneuvering motion are shown in Equation 10.

$$\begin{aligned}
&\left(m+m_x\right)\cdot\dot{u}-m\cdot\left(v\cdot r+x_G\cdot r^2\right)\\
&=X_H+X_P+X_R+R(u)\\
&\left(m+m_y\right)\cdot\dot{v}+\left(m\cdot x_G+m_y\cdot x_r\right)\cdot\dot{r}+m\cdot u\cdot r\\
&=Y_H+Y_R \qquad (10)\\
&\left(I_{zz}+m\cdot x_G^2+J_{zz}+m_y\cdot x_r^2\right)\cdot\dot{r}\\
&+\left(m\cdot x_G+m_y\cdot x_r\right)\cdot\dot{v}+m\cdot x_G\cdot u\cdot r\\
&=N_H+N_R
\end{aligned}$$

Right side in the equation 10 are the external forces X, Y and moment N consisting of hull, propeller and rudder components. $R(u)$ of the ship with the MVT rudder which was used in the simulation was measured by resistance test in the towing tank. Figure 14 shows the coordinate system and the definition of various parameters.

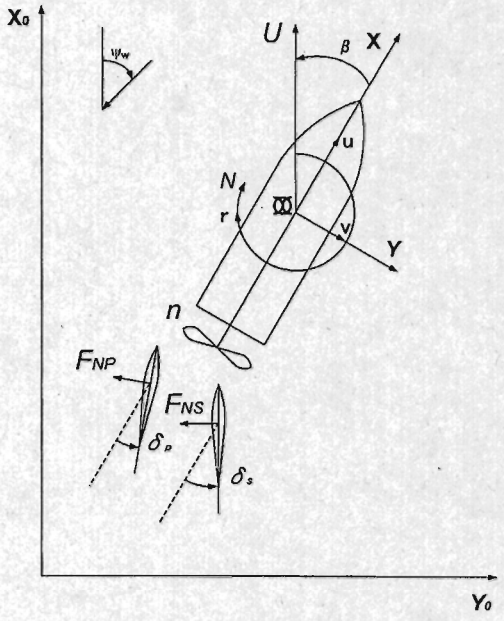

Fig.14 Coordinate system

For estimating the hull forces and moment, Equations 11 -13 were used. Hydrodynamic coefficients such as ax2 , dn2 etc are estimated based on Kang's regression formula [8].

$$\begin{aligned}
X'_H &= (\mathrm{ax2}\cdot\sin^2(\beta)+\mathrm{ax4}\cdot\sin^2(2\beta))\cdot\cos(\beta)\\
&+\mathrm{bx1}\cdot\sin(\beta)\cdot r'\\
&+\mathrm{bx2}\cdot\sin(2\beta)\cdot r'\cdot\mathrm{sign}(\cos(\beta)) \qquad (11)\\
Y'_H &= (\mathrm{ay1}+\mathrm{cy1}\cdot r'^2)\cdot\sin(\beta)\\
&+\mathrm{ay3}\cdot\sin(3\beta)+\mathrm{ay5}\cdot\sin(5\beta) \qquad (12)\\
&+\left(\mathrm{dy1}\cdot r'+\mathrm{ey1}\cdot r'^3\right)\cdot\cos(\beta)\\
N'_H &= (\mathrm{an2}+\mathrm{cn2}\cdot r'^2)\cdot\sin(2\beta)\\
&+\mathrm{an4}\cdot\sin(4\beta)+\mathrm{dn0}\cdot r' \qquad (13)\\
&+\mathrm{en0}\cdot r'^3+\mathrm{dn2}\cdot r'\cdot\cos(2\beta)
\end{aligned}$$

The estimated coefficients were corrected from the comparison of the results between the free running experiment and the simulation to increase accuracy of the simulation. The maximum allowable variation of hydrodynamic coefficient was set as 15% of the original value. Figure 15 and Figure 16 show the comparisons between the results of the simulation after modifying the hydrodynamic coefficients and those of the free running experiment. The time

histories of heading angle and rudder angle of both the simulations and the experiments matched well at 10 degrees and 20 degrees Zigzag tests in Figure 15. On the comparison of the velocity components in Figure 16, the simulations of the Zigzag tests have also good agreements with those of the experiment. At -30 degrees Turning Tests in Figure 15, there are some discrepancies between the trajectories from the simulation and the experiment, but turning circle diameter which represents the maneuverability in steady turning had similar values. The simulation of Turning test also well described the velocity components of the experiment in Figure 16. The modified coefficients may not have optimum values for the VLCC model ship because of the apparent discrepancy in the turning test. However, the established simulation model with the modified coefficients was considered to be suitable for use in the next stage of analysis.

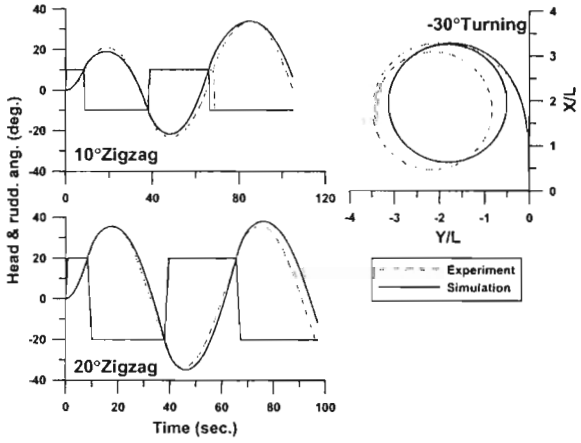

Fig.15 Comparisons of Zigzag and turning tests between experiment and simulation

4. VIRTUAL ZERO RUDDER ANGLE

As mentioned in section 2.3, the inflow angle to each rudder is not parallel to the longitudinal direction of the ship. This means that when both rudders are positioned in parallel at small angles below δ_{S0} or δ_{P0}, the lift force from each rudder acts in the opposite direction on the hull. This phenomenon can be a factor which reduces the maneuverability of the ship at small rudder angles. One way to solve this problem is by setting each rudder at an angle as corresponding to the inflow angle to the rudder. Both the rudders are operated from the virtual zero rudder angle. The above setting is defined as virtual zero rudder angle. The sketch of this concept is shown in Figure 17.

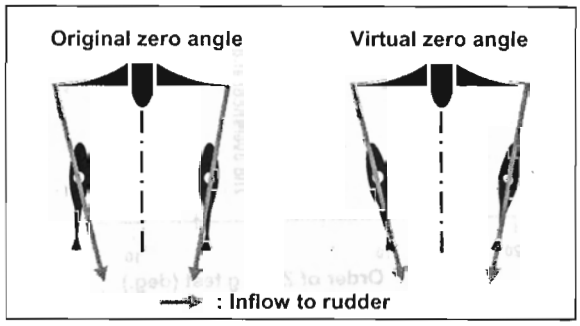

Fig.17 Concept of virtual zero rudder angles

Several simulations were carried out to show the difference of the operations between using the original zero rudder angle and virtual zero rudder angle. Two type of the virtual rudder angles were simulated for Zigzag simulation and Reverse Spiral simulation. One type had constant angles that were set 4.6 degrees for the port side rudder and -4.8 degrees for the starboard side rudder. The other type had controllable angle corresponding to δ_{S0} or δ_{P0} which are varied with S.

Eight sets of Zigzag simulations were carried out with the different type of virtual zero rudder angle. The results of the simulations are shown with first and second overshoot angle in Figure 18. There is not much difference in the first overshoot for port side

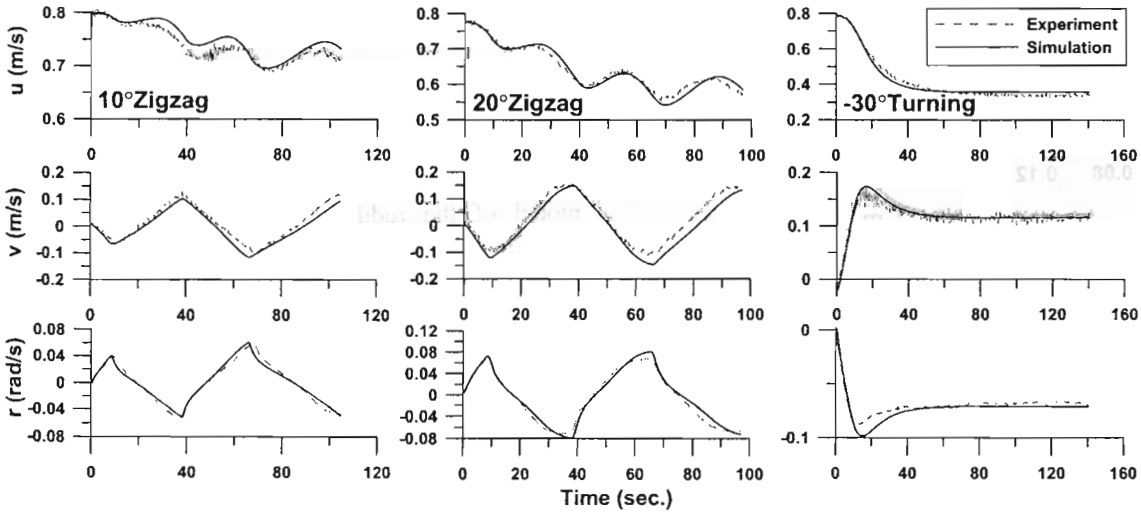

Fig.16 Comparisons of time histories between experiment and simulation

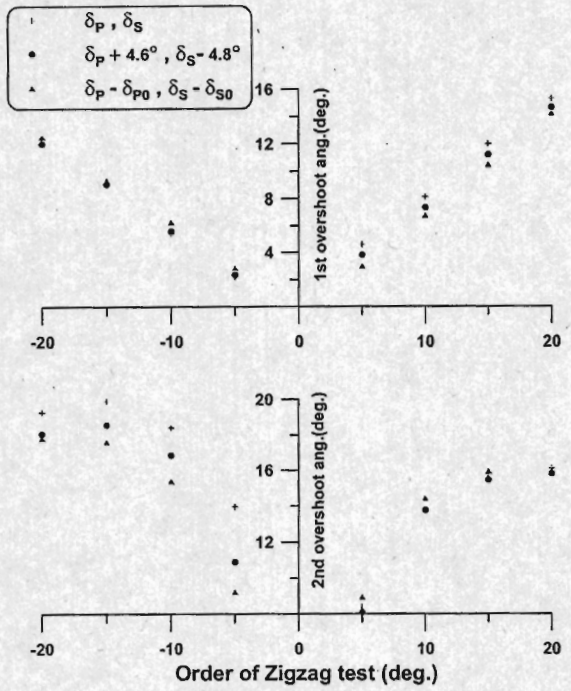

Fig.18 First and second overshoot angle

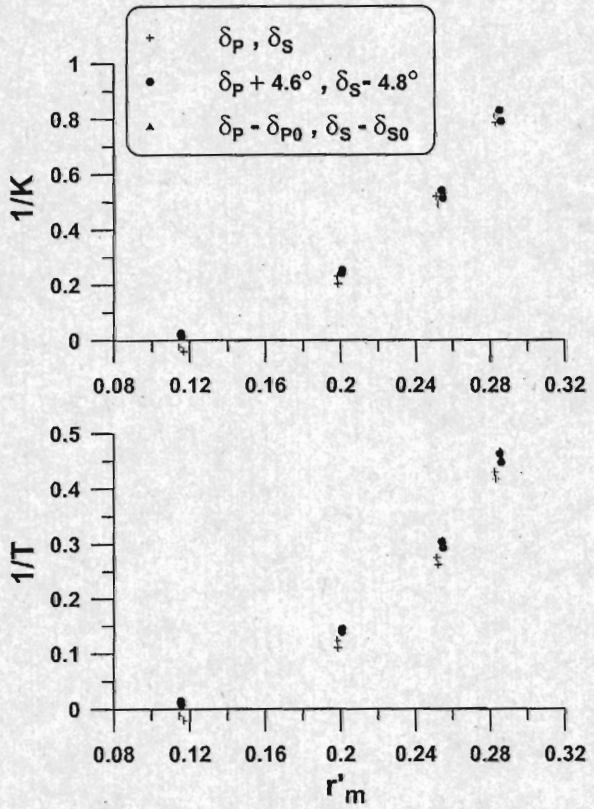

Fig.19 Comparison of K' and T' in Zigzag simulations

Zigzag tests and the second overshoot angle for starboard side Zigzag test. On the contrary, it was observed that the first overshoot angles for starboard side Zigzag test were reduced when using the virtual zero rudder angle, moreover the disparity in the second overshoot angles for port side Zigzag test is getting larger. Nomoto's indexes [9] K', T' were plotted as functions of r'_m, in Figure 19. It is well known that K' demonstrates the turning ability of a ship and T' demonstrates the course stability. Generally the simulation using the virtual zero angles has better turning ability and course stability compared to that with the original zero angle.

Figure 20 shows the results of the Reverse spiral simulation with small rudder angle. The Reverse spiral tests can draw the loop width which is one of the indexes for coursekeeping ability. When using the virtual zero rudder angle, the loop width are also reduced as compared to using the original zero rudder angle. The advantage of using the varied virtual zero angle is that it not only reduces the overshoot angle and the loop width, but also asymmetrical maneuvering motions. However, the concept of the variable virtual zero angle may be difficult to implement in real operation, because it may additional special sensing equipment. It may be noted that only using the constant virtual zero angle also has the better maneuverability as compared to the original zero angle, and this concept is easy to apply to the real operation.

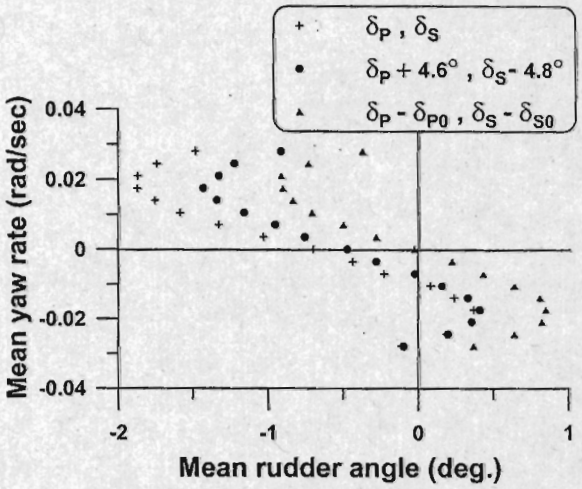

Fig.20 Loop width from Reverse spiral simulations

5. CONCLUSION

This paper describes the performance of a MVT rudder installed in a large vessel. The mathematical model of the rudder is developed based on the experiment data by carrying out self propulsion tests on a VLCC model ship. A virtual zero angles of the MVT rudder is proposed to improve the maneuverability of a blunt-body ship installed with the MVT rudder.

(1) The self propulsion experiments were carried out to examine the performance of the MVT rudder which is installed in the VLCC model ship. It is observed that the value of the inflow angle to the

MVT rudder can not be neglected as in case of conventional mariner rudder.

(2) The mathematical model of the MVT rudder is in the form of a function which outputs inflow speed to each side rudder as per the rudder angle. The model was validated by comparing the results of the calculation with the developed model to that of the experiment.

(3) Simulations of the VLCC with an MVT rudder using the developed rudder model were carried out and modified by comparing to the results of the free running tests. In cases of the simulation utilizing the virtual zero rudder angle, it is observed that the maneuverability of the VLCC installed with MVT rudder was improved as compared to the original simulation which use the original zero rudder angle.

ACKNOWLEDGEMENT

This study is a part of the subsidizing project of the "Ship & Ocean Foundation" in 2003 with the title "Research & Development on a Single Shaft Twin High Lift Rudders System for Large Vessels".

REFERENCES

[1] IMO MSC 76/23 "Resolution MSC.137(76), standards for ship manoeuvrability", Report of the maritime safety committee on its seventy-sixth session-annex 6, 2002

[2] Nabeshima K, Omote M, Ueno A, et al "A new type rudder, "Vectwin" and the actual results of its manoeuvring performance" (in Japanese), J Kansai Soc Nav Archit, 228, pp.157-165, 1997

[3] Hasegawa K, Kang D H, Sano M,et al "A Study on the Maneuverability of a Large Vessel Installed with a Mariner Type Super Vec-twin Rudder", J Mar Sci Technol, 11-2, 2006

[4] Hamamoto M, Enomoto T "Maneuvering performance of a ship with Vec twin rudder system", J Soc Nav Archit Jpn, 181, pp197-204, 1997

[5] Fujii H "A consideration on ship-model correlation in ship manoeuvrability", Trans West Jpn Soc Nav Archit, 62, 1981

[6] DNV "Hull equipment and appendages: stern frames, rudders and steering gears. Rules for classification steel ships", part3 chapter 3 section 2, pp.2-19, 1985

[7] Kose K, Hosokawa M, Yamada H, et al "A study on performance estimation of special rudders "(in Japanese), Trans West Jpn Soc Nav Archit, 84, pp.49-57, 1992

[8] Kang D H, Hasegawa K "A practical prediction method of hydrodynamic forces acting on the hull of a blunt-body ship", Conf Proc JASNAOE, 1, pp.219-220, 2005

[9] Nomoto K, Karasuno K "A new procedure of maneuvering model experiment" (in Japanese), J Soc Nav Archit Jpn, 126, pp.131-140, 1969

LIST OF SYMBOLS

a_H ratio of hydrodynamic force induced on ship hull by rudder action to rudder force
A_R rudder area
B ship breadth
C_b block coefficient
d ship draft
D_P propeller diameter
F_{NS}, F_{NP} rudder normal force for starboard and port rudder respectively
$J_P = (1-\omega_P)u / nD_P$ propeller advance coefficient
$J_S = u / nD_P$ advance ratio
K' Nomoto's index which is related to turning ability
L ship length
m ship mass
m_x added mass in surge
m_y added mass in sway
n propeller revolution
O ship's center of gravity
P propeller pitch
r yaw rate
r'_m non-dimensional mean angular velocity as defined by Nomoto for Zigzag test.
$R(u)$ ship resistance
$S = 1-(1-\omega_P)u / nP$ slip ratio
S_W wetted surface area
T' Nomoto's index which is related to course stability
t_P thrust deduction factor
t_R coefficient for additional drag of rudder
u surge velocity
U ship velocity
v sway velocity
x_G distance between ship's center of gravity and ship's center
x_H ratio of hydrodynamic moment induced on ship hull by rudder action to rudder force
α_{RS}, α_{RP} starboard and port effective rudder inflow angle
β drift angle
δ_S, δ_P starboard and port rudder angles
ε wake ratio between propeller and rudder
ρ water density
ω_P effective wake fraction

AUTHOR'S BIOGRAPHY

Dong-Hoon Kang received the M.Sc. degree in Naval Architecture & Ocean Engineering from Pusan National University in 2003. He is currently working as a Ph.D. student in the field of Naval Architecture at Osaka University. He has been engaged in

researches on Low speed maneuvering, special rudder system and automatic control of ship.

Kazuhiko Hasegawa is a professor at Osaka University in Japan. He was a member of several international technical / editorial committees. Hasegawa has been conducting dozens of projects relating to collision avoidance, automatic berthing, marine simulator and maritime traffic simulation.

Kenjiro Nabeshima is vice president of Japan Hamworthy Co. Ltd. He graduated from Tokyo University and worked at Hitachi Zosen Corp. for approximately 40 years. After joining Japan Hamworthy Co. Ltd. he has been engaged in the design of special type rudder and steering gear such as VL vec-twin rudder and schilling rudder.